

Deep ultraviolet emission from ultra-thin GaN/AlN heterostructures

Dylan Bayerl,^{1,a)} SM Islam,^{2,a)} Christina M. Jones,³ Vladimir Protasenko,² Debdeep Jena,^{2,b)} and Emmanouil Kioupakis^{1,c)}

¹Department of Materials Science and Engineering, University of Michigan, Ann Arbor, Michigan 48109, USA

²Department of Electrical and Computer Engineering, Cornell University, Ithaca, New York 14853, USA

³Applied Physics Program, University of Michigan, Ann Arbor, Michigan 48109, USA

(Received 8 August 2016; accepted 23 November 2016; published online 16 December 2016)

We present the theoretical and experimental results for the electronic and optical properties of atomically thin (1 and 2 monolayers) GaN quantum wells with AlN barriers. Strong quantum confinement increases the gap of GaN to as high as 5.44 eV and enables light emission in the deep-UV range. Luminescence occurs from the heavy and light hole bands of GaN yielding $E \perp c$ polarized light emission. Strong confinement also increases the exciton binding energy up to 230 meV, preventing a thermal dissociation of excitons at room temperature. However, we did not observe excitons experimentally due to high excited free-carrier concentrations. Monolayer-thick GaN wells also exhibit a large electron-hole wave function overlap and negligible Stark shift, which is expected to enhance the radiative recombination efficiency. Our results indicate that atomically thin GaN/AlN heterostructures are promising for efficient deep-UV optoelectronic devices. Published by AIP Publishing. [<http://dx.doi.org/10.1063/1.4971968>]

The group-III-nitrides are important semiconductors for light emitting diodes (LEDs) and lasers. AlN and GaN quantum wells (QWs) emit light in the ultraviolet (UV) range, due to their bulk electronic gaps of 6.2 eV and 3.4 eV, respectively. The deep-UV range (4.4–5.4 eV) is particularly important for optical sterilization and germicidal applications.¹ Efforts to achieve a deep-UV emission from III-nitrides focus on structures with high-Al-content AlGaIn QWs grown along the polar c -axis direction.² Attaining high electricity-to-light conversion efficiency with this approach has proven difficult. Reasons include the challenges of achieving p-type AlGaIn,³ efficiency loss from polarization fields and the quantum-confined Stark effect,⁴ and poor light extraction due to AlN-like polarization of emitted light.⁵

Heterostructures of ultra-thin GaN wells with AlN barriers (Fig. 1) are alternatives to AlGaIn alloys for deep-UV emission. Extreme quantum confinement in wells only a few atomic monolayers (MLs) thick increases the electronic gap of GaN by several electron volts and achieves a light emission in the deep-UV.^{6–8} This configuration preserves $E \perp c$ polarized light emission. In c -plane-grown devices such as that shown schematically in Fig. 1, $E \perp c$ light is emitted from the exposed c -plane surface, enabling an efficient light extraction from the device, which has previously been demonstrated theoretically⁶ and experimentally.⁷ In contrast, high-Al-content AlGaIn wells emit $E \parallel c$ light in the plane of the device, which reduces light extraction efficiency. Furthermore, ultra-thin GaN wells mitigate the polarization-field-induced separation of electrons and holes, which has been theorized to improve the radiative efficiency,⁹ as well as minimize the Stark shift.

In this work, we present a theoretical and experimental study of the electronic and optical properties of atomically thin GaN/AlN heterostructures. We use many-body perturbation

theory to predict the accurate electronic and optical gaps including excitonic effects. Furthermore, we model the photoluminescence (PL) spectrum and compare to experimental measurements. Our results for the optical properties exhibit an excellent agreement between theory and experiment.

Pioneering theoretical work by Kamiya *et al.* previously considered the electronic band gap and optical polarization properties of ultra-thin GaN/AlN heterostructures for deep-UV emitters.⁶ We build on their work by calculating accurate quasiparticle corrections to predict the band gap, rather than employing a scissors-shift operator to adjust the gap.

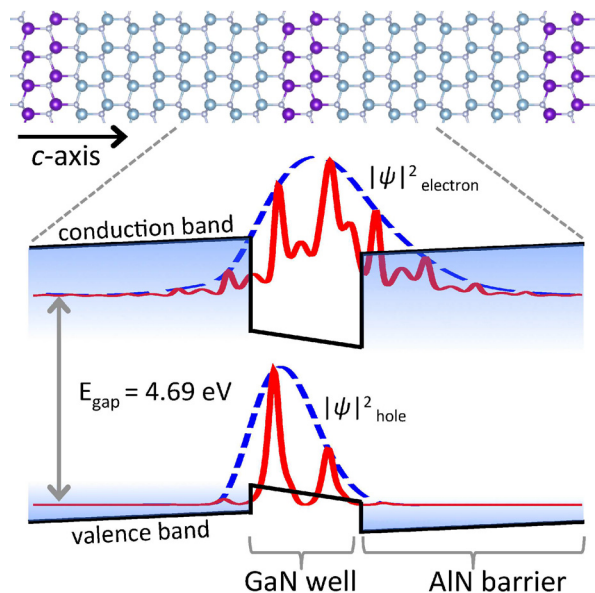


FIG. 1. Structure and band diagram of an ultra-thin GaN/AlN heterostructure grown along the c -axis with 2 ML GaN wells separated by 8 MLs of AlN. Quantum confinement increases the electronic gap (E_{gap}) into the deep UV range, e.g., the indicated value of 4.69 eV for the structure shown. Electron and hole wave functions ($|\psi|^2$ solid lines) are strongly localized by the thin GaN well. Polarization fields separate and reduce the overlap of the envelope functions ($|\psi|^2$ dashed lines).

^{a)}D. Bayerl and S. M. Islam contributed equally to this work.

^{b)}Electronic mail: djena@cornell.edu.

^{c)}Electronic mail: kioup@umich.edu.

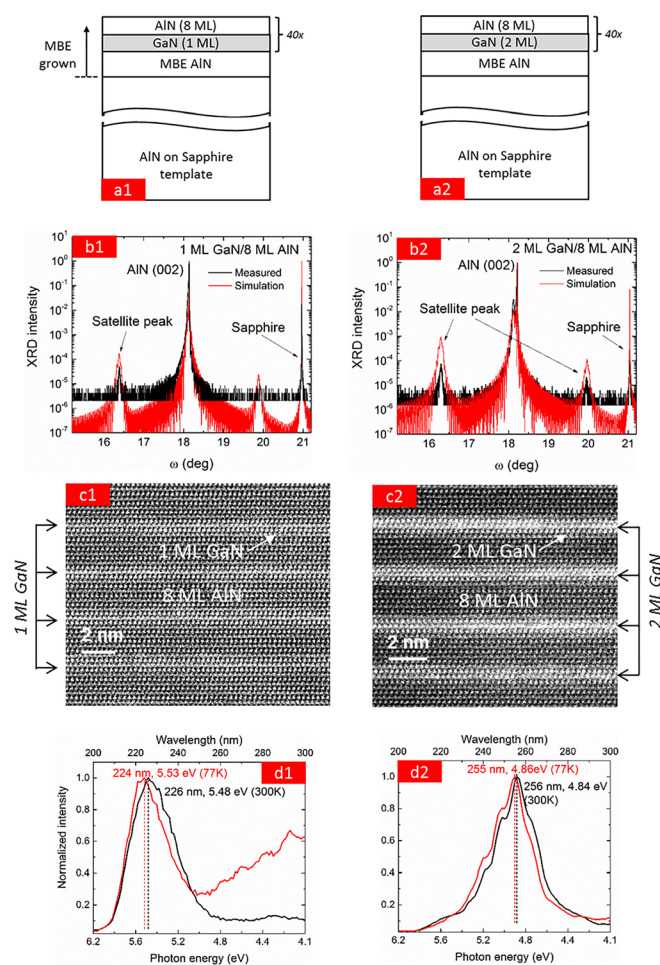


FIG. 2. Schematic of GaN/AiN heterostructure samples (a). Simulated and measured XRD $\omega - 2\theta$ triple axis scans showing superlattice fringes on the AlN (002) peak and satellite peaks from GaN wells (b). STEM image showing insertion of GaN wells between AlN barriers (c). Experimental PL spectra with photon energies of peak intensity indicated (d).

Additionally, we predict the excitonic properties of ultra-thin GaN/AiN, which have not been previously investigated using accurate first-principles methods.

We use first-principles methods based on density functional and many-body perturbation theory, which yield accurate electronic and optical properties of materials.¹⁰ We calculated the electronic (quasiparticle) gaps with the G_0W_0 (GW) method, and optical gaps (lowest exciton energies) with the Bethe-Salpeter equation (BSE) method using the Quantum ESPRESSO,¹¹ BerkeleyGW,¹² and Wannier90¹³ codes (details in [supplementary material](#)).

To experimentally test our theory predictions, we grew and characterized a series of ultra-thin GaN/AiN heterostructures via molecular beam epitaxy (MBE). Growth details are in the [supplementary material](#). Schematics of the grown structures are shown in Fig. 2(a). Eleven samples were grown with 1 ML or 2 MLs thick GaN wells and AlN barrier thickness from 7 to 16 MLs. We used 40 periods of GaN/AiN layers to strengthen the PL signal. Growth of structures with AlN barriers thinner than 7 MLs was attempted, but TEM observations show that GaN-AiN intermixing took place for such thin barriers, precluding comparison to our theoretical calculations for structures with sharp heterointerfaces. After the MBE growth, we performed X-ray

diffraction (XRD) $\omega - 2\theta$ triple axis scans to check the formation of superlattice fringes. All samples show such fringes around the central (002) AlN peak, as well as the satellite peaks from GaN layers (Fig. 2(b)). The satellite peak spacing differs between 1 ML GaN/8 ML AlN and 2 ML GaN/8 ML AlN samples due to the difference in the average GaN content, which is 11% and 20%, respectively. Simulations of the XRD spectra using structural parameters from our theoretical calculations are in good agreement with the experimentally measured spectra. TEM analyses were performed on the samples to investigate the crystallinity and layer structure (Fig. 2(c)). Thicknesses of GaN wells and AlN barriers are consistent with the desired values, deviating by 1 ML at most for the AlN layers.

To characterize the optical properties, PL measurements were performed at 300 K and 77 K with a 157 nm (7.89 eV) pulsed excimer laser source (additional details in [supplementary material](#)). Fig. 2(d) shows representative examples of the measured spectra. The emission spectra blueshift by approximately 0.05 to 0.1 eV as the temperature was reduced, comparable to the 0.07–0.09 eV shift predicted by Varshni's law for the bulk materials.¹⁴ The photon energies of PL intensity peaks are shown in Fig. 3(a). Our experimental PL data are in good agreement with the reported emission energies for MOCVD-grown ultra-thin GaN/AiN superlattices. Taniyasu and Kasu reported 5.23 eV emission for a 0.9 ML GaN/7.2 MLs AlN structure and 4.84 eV emission for a 1.8 MLs GaN/7.3 MLs AlN structure.⁷ For similar configurations (1 ML GaN/7 MLs AlN and 2 MLs GaN/8 MLs AlN), we observed the PL peaks at 5.32 eV and 4.84 eV, respectively. While $E \perp c$ polarized PL has previously been predicted⁶ and measured⁷ in similar structures, constraints of our PL apparatus preclude the measurement of edge-emission from our samples.

Next, we compare our experimental data to our theoretical predictions. The electronic and optical gaps are shown in Fig. 3(a). We calculated the gaps of ultra-thin GaN/AiN heterostructures for nine structures, with GaN wells 1 ML or 2 MLs thick and AlN barriers 1 ML to 9 MLs thick. For the thinnest 1 ML GaN well separated by 9 MLs AlN, quantum confinement increases the electronic gap to 5.44 eV. Thicker barriers increase the electronic gap of 1-ML wells only slightly above this value (Fig. 3(a)). At the other extreme, the structure of alternating GaN and AlN single MLs has an electronic gap of 4.76 eV, which is comparable to the average electronic gap of bulk GaN and AlN. Figure 3(a) also shows that the electronic gaps decrease by almost 0.7 eV when increasing the GaN well width from 1 ML to 2 MLs for AlN barriers thicker than 5 MLs thick. Additionally, the Stark shift influences the electronic gaps of the 2-ML GaN structures. For 2 ML GaN wells and the AlN barriers thicker than 4 MLs, the electronic gap is approximately constant even though thicker barriers should increase the gap by increasing confinement, as observed for 1 ML GaN wells. The expected electronic gap increase in 2 ML GaN structures is offset by an increasing Stark shift (inset Fig. 3(b)). This effect is not observed in 1 ML GaN structures since the Stark shift is suppressed by the strong confinement.

We also calculated the effective masses of the quasiparticle band structures (see [supplementary material](#)). We found that the effective masses in ultra-thin GaN/AiN

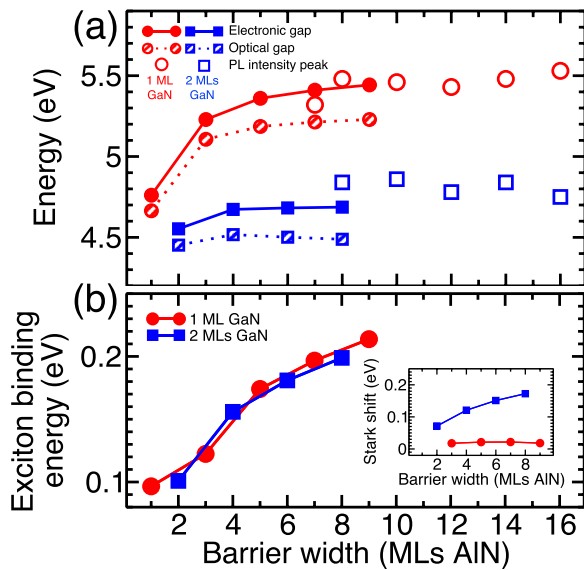


FIG. 3. Electronic and optical gaps of ultra-thin GaN/AlN heterostructures as a function of the well (MLs GaN) and barrier (MLs AlN) thickness (a). Experimentally measured PL peaks at 300 K are indicated with open symbols. The calculated exciton binding energy (b) and Stark shift magnitude (inset) as a function of well and barrier thickness. Lines connecting the theory data points are guides to the eye.

heterostructures are larger for electrons and smaller for holes than bulk GaN and AlN, which we attribute to biaxial compressive strain in the ultra-thin GaN layer.¹⁵

The calculated optical gaps (Fig. 3(a)) show that deep-UV emission is possible with GaN wells with a thickness of 1 ML (4.66–5.23 eV) or 2 MLs (4.45–4.52 eV). For 2 ML GaN structures, the optical gap decreases as the barrier thickness increases above 4 MLs of AlN due to the strong dependence of the exciton binding energy on the barrier thickness (Fig. 3(b)). The strong confinement in ultra-thin GaN results in large exciton binding energies between 96 meV and 230 meV, much larger than the bulk materials. Such large exciton binding energies exceed $k_B T$ at room temperature and can result in excitonic recombination.¹⁶ Increasing the barrier thickness enhances the exciton confinement, increases the binding energy, and reduces the optical gap. This effect is most apparent in structures with 2 ML GaN wells in which the Stark shift offsets the confinement-induced increase of the electronic gap (Fig. 3(a)). The fundamental optical transition involves the heavy and light hole bands, resulting in $E \perp c$ polarized light emission (see [supplementary material](#)).

Comparison of experimentally measured PL peak energies to calculations (Fig. 3(a)) reveals that PL peaks are closer to the electronic than optical gaps. Therefore, despite the large exciton binding energies, emission in our PL measurements is non-excitonic. Exciton formation is likely suppressed due to screening of the Coulomb attraction between electrons and holes by free carriers. Our calculations include the screening by the valence electrons, but not the additional screening caused by phonons or free carriers. The large exciton binding energies (~ 200 meV) in the ultra-thin structures are much higher than the GaN LO phonon energy (94 meV),¹⁷ indicating that phonons are too slow to screen the excitons. However, the additional screening by free carriers can significantly reduce the exciton binding energy and

make it comparable to the LO phonon energy. Phonons then screen and weaken the Coulomb interaction even further, decreasing the binding energy and increasing the radius of excitons, which lowers the Mott critical density. Our estimates indicate that the exciton density may exceed the Mott critical density under our experimental conditions, causing exciton dissociation. The carrier screening length is computed via the Thomas-Fermi model for degenerate electrons and the Debye model for non-degenerate holes.¹⁸ In our 1 ML and 2 ML GaN structures at 300 K, a carrier density of $n = p = 5 \times 10^{19} \text{ cm}^{-3} = 1.2 \times 10^{13} \text{ cm}^{-2}$ (as estimated from PL measurements discussed below) yields a free-carrier screening length of 0.2 nm. This reduces the effective binding energy by approximately 45%,¹⁹ whereupon, the LO phonons screen excitons even further and cause them to dissociate. Lowering the temperature increases the effectiveness of Debye screening, so excitons still do not appear in our PL measurements at 77 K. We also predict that for a free-carrier density of $5 \times 10^{18} \text{ cm}^{-3}$, typical of commercial nitride LEDs at peak efficiency, excitons are not screened and excitonic recombination is possible at room temperature.

The PL emission spectra also show a significant broadening (0.3–0.4 eV, Fig. 4). We also estimate the broadening due to carrier occupation and structural disorder from the slope of the logarithm of the PL high-energy tail (Fig. 4(a)).²⁰ The occupational-structural broadening parameter for 2 ML GaN wells is 0.22–0.32 eV, but for 1 ML GaN structures wells, there is no well-defined linear region in the PL spectra.

Next, we model the non-excitonic PL spectra and compare the predicted peak positions and lineshapes with experiment for structures with AlN barriers 8 to 9 MLs thick. Steady-state PL for QWs is modeled with the Shockley – van Roosbroeck (SvR) equation,²¹ $I_{\text{well}}(E) \propto E^3 f_e f_h \sqrt{-\epsilon_1 + \sqrt{\epsilon_1^2 + \epsilon_2^2}}$, which yields the relative PL intensity I_{well} at photon energy E using the electron f_e and hole f_h Fermi occupations and the complex dielectric function $\epsilon_1 + i\epsilon_2$. The Fermi occupations are calculated using the first-principles density of states. The non-excitonic dielectric functions include a Lorentzian spectral broadening parameter Γ .¹² The occupational-structural broadening Δ , carrier densities n and p , and spectral broadening Γ are used as parameters to fit to experimental data. Excellent agreement between the SvR model and experiment is obtained for the lineshape and peak position of the 2 ML GaN structure (Fig. 4(b)), with a choice of fitting parameters of $n = p = 5 \times 10^{19} \text{ cm}^{-3} = 1.2 \times 10^{13} \text{ cm}^{-2}$, $\Delta = 0.22$ eV, and $\Gamma = 0.08$ eV. This occupational-structural broadening is within the range estimated from Fig. 4(a), while the carrier density is within the range expected during our PL experiments. Multiple shoulder peaks in the high-energy tail of the PL spectrum are due to peaks in the dielectric function, rather than the Fermi occupation of additional subbands.

In contrast to 2 ML GaN, the QW model disagrees with the experimental PL data for the 1 ML GaN structure (Fig. 4(c)). Though the experimental PL lineshape can be approximated by the QW model, the predicted peak position is too high. No combination of model parameters yields a good agreement with both the experimental peak position and lineshape. The parameters of the QW PL model in Fig. 4(c) are $n = p = 3 \times 10^{20} \text{ cm}^{-3} = 7.4 \times 10^{13} \text{ cm}^{-2}$, $\Delta = 0.09$ eV, and

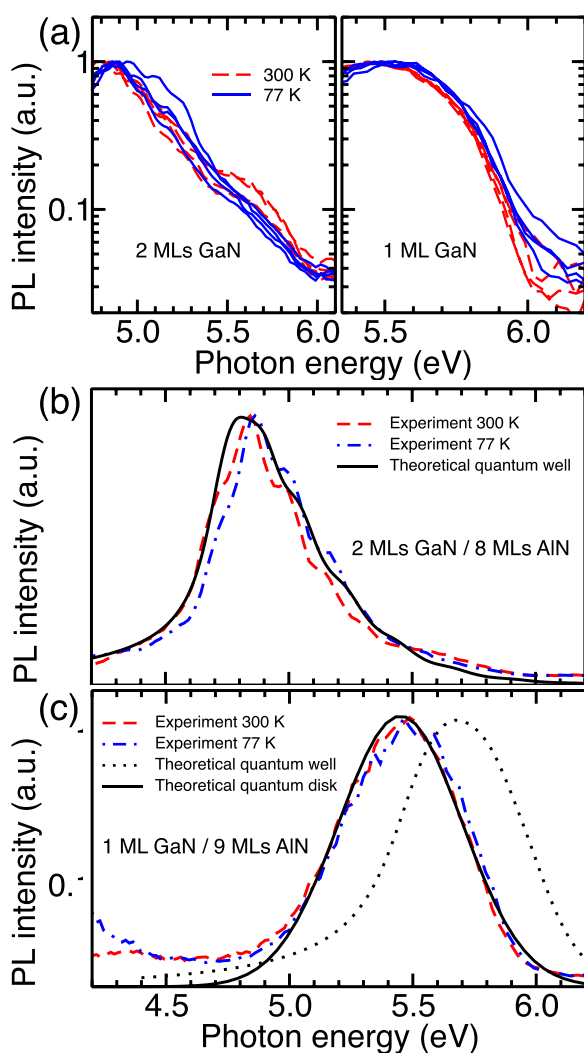


FIG. 4. Semi-log plots of high-energy tails of experimental PL spectra of ultra-thin GaN/AiN heterostructures. Experimental and modeled PL spectra for heterostructure with 2 ML GaN (b). Modeling 2 ML GaN PL as a QW (solid line) matches the experimental peak position and lineshape. Experimental and modeled PL spectra for heterostructure with 1 ML GaN (c). Modeling the 1 ML GaN structure as a quantum disk (solid black line) agrees much better with the experiment than the QW PL model (dotted black line).

$\Gamma = 0.16$ eV. These parameters differ considerably from the fit for 2 ML GaN. The overall poor fit to the experimental PL spectrum indicates that 1 ML GaN samples do not luminesce as QWs, but rather as quantum disks with homogeneously broadened emission at the electronic gap energy.²² Figure 3(a) supports this conclusion, since the PL peak energies are in close agreement with the calculated electronic gaps. Indeed, modeling the PL spectrum of 1 ML GaN as a quantum disk yields excellent agreement with experiment (Fig. 4(c)). The quantum disk model is $I_{\text{disk}}(E) \propto (1/\sigma)e^{-(E-E_g)^2/2\sigma^2}$, where the peak position and lineshape of the relative luminescence intensity I_{disk} that are governed by the electronic gap E_g and broadening parameter σ . The quantum disk model of the PL spectrum assumes that the quantum confinement arises predominantly from the ultra-thin out-of-plane direction while the in-plane confinement effects are negligible. Thus, the density of states is sharply peaked at the band edges. The fitted value for the broadening parameter is $\sigma = 0.25$ eV, which we attribute to fractional GaN monolayer formation.²³

The different PL characteristics of 1 ML and 2 ML structures are explained by the growth kinetics of the ultra-thin GaN layer. Any deviation from the ideal monolayer coverage results in fractional monolayer formation, as observed in ultra-thin InN/GaN heterostructures.²⁴ Therefore, fractional 2 ML growth yields a full ML plus a fractional second ML, while the fractional 1 ML growth yields epitaxial GaN disks.²⁵ Thus, 1 ML GaN layers behave as isolated quantum disks while 2 ML GaN layers behave as QWs since GaN coverage is continuous.

The formation of fractional monolayers is also indicated by the observed broadening of the PL spectrum. To verify the origin of the broadening, we performed $k \cdot p$ calculations using nextnano²⁶ to model QWs containing fractional GaN monolayers with GaN disk diameters ranging from 5–10 nm. For a carrier density of $1.2 \times 10^{13} \text{ cm}^{-2}$ obtained from our PL modeling, the energy range of occupied free-carrier states is 0.30–0.43 eV, which is consistent with the PL broadening measured experimentally in 1 ML and 2 ML GaN structures. Therefore, monolayer thickness fluctuations with a lateral scale of 5–10 nm explain the observed PL broadening.

In conclusion, we grew, characterized, and calculated the ultra-thin GaN/AiN heterostructures to elucidate their electronic and optical properties. Extreme quantum confinement enables light emission in the germicidal deep-UV range. We also predict large exciton binding energies which allow stable excitons at room temperature. However, the high excited carrier density in PL precluded the direct observation of excitons. 1 ML structures have the characteristics of quantum disks and 2 ML structures behave as QWs. Our work indicates that ultra-thin GaN/AiN heterostructures have excellent features for applications in deep-UV optoelectronics.

See [supplementary material](#) for details of first-principles calculation methods, details of sample growth and characterization techniques, electronic band structures and calculated effective masses of selected heterostructures, and exciton binding energies of heterostructures with thicker GaN wells.

This work was supported by the NSF DMREF program under Award Nos. 1534221 and 1534303. D.B. was supported by the J. Robert Beyster Computational Innovation Graduate Fellowship. Computational resources were provided by the DOE NERSC facility (DE-AC02-05CH11231).

¹J. Jagger, *Introduction to Research in Ultraviolet Photobiology* (Prentice-Hall, Englewood Cliffs, N.J., 1967).

²Y. Taniyasu, M. Kasu, and T. Makimoto, *Nature* **441**, 325 (2006).

³J. Simon, V. Protasenko, C. Lian, H. Xing, and D. Jena, *Science* **327**, 60 (2010).

⁴J. Speck and S. Chichibu, *MRS Bull.* **34**, 304 (2009).

⁵R. Banal, M. Funato, and Y. Kawakami, *Phys. Rev. B* **79**, 121308 (2009).

⁶K. Kamiya, Y. Ebihara, K. Shiraishi, and M. Kasu, *Appl. Phys. Lett.* **99**, 151108 (2011).

⁷Y. Taniyasu and M. Kasu, *Appl. Phys. Lett.* **99**, 251112 (2011).

⁸J. Sellés, C. Brimont, G. Cassabois, P. Valvin, T. Guillet, I. Roland, Y. Zeng, X. Checoury, P. Boucaud, M. Mexis *et al.*, *Sci. Rep.* **6**, 21650 (2016).

⁹E. Kioupakis, Q. Yan, and C. G. Van de Walle, *Appl. Phys. Lett.* **101**, 231107 (2012).

¹⁰J. M. Rondinelli and E. Kioupakis, *Annu. Rev. Mater. Res.* **45**, 491 (2015).

¹¹P. Giannozzi, S. Baroni, N. Bonini, M. Calandra, R. Car, C. Cavazzoni, D. Ceresoli, G. L. Chiarotti, M. Cococcioni, I. Dabo, A. D. Corso, S. de Gironcoli, S. Fabris, G. Fratesi, R. Gebauer, U. Gerstmann, C.

- Gougoussis, A. Kokalj, M. Lazzeri, L. Martin-Samos, N. Marzari, F. Mauri, R. Mazzarello, S. Paolini, A. Pasquarello, L. Paulatto, C. Sbraccia, S. Scandolo, G. Sclauzero, A. P. Seitsonen, A. Smogunov, P. Umari, and R. M. Wentzcovitch, *J. Phys.: Condens. Matter* **21**, 395502 (2009).
- ¹²J. Deslippe, G. Samsonidze, D. A. Strubbe, M. Jain, M. L. Cohen, and S. G. Louie, *Comput. Phys. Commun.* **183**, 1269 (2012).
- ¹³A. A. Mostofi, J. R. Yates, Y.-S. Lee, I. Souza, D. Vanderbilt, and N. Marzari, *Comput. Phys. Commun.* **178**, 685 (2008).
- ¹⁴N. Nepal, J. Li, M. Nakarmi, J. Lin, and H. Jiang, *Appl. Phys. Lett.* **87**, 242104 (2005).
- ¹⁵C. Dreyer, A. Janotti, and C. Van de Walle, *Appl. Phys. Lett.* **102**, 142105 (2013).
- ¹⁶T. Langer, A. Chernikov, D. Kalincev, M. Gerhard, H. Bremers, U. Rossow, M. Koch, and A. Hangleiter, *Appl. Phys. Lett.* **103**, 202106 (2013).
- ¹⁷G. Callsen, G. M. Pahn, S. Kalinowski, C. Kindel, J. Settke, J. Brunmeier, C. Nenstiel, T. Kure, F. Nippert, A. Schliwa *et al.*, *Phys. Rev. B* **92**, 235439 (2015).
- ¹⁸H. Ibach and H. Lüth, *Solid-State Physics: An Introduction to Principles of Materials Science*, 4th ed. (Springer-Verlag, 2010), pp. 151–152.
- ¹⁹E. R. Vrscaj, *Phys. Rev. A* **33**, 1433 (1986).
- ²⁰J. A. Ferrer-Pérez, B. Clafin, D. Jena, M. Sen, R. Vetry, and D. Dorsey, *J. Electron. Mater.* **43**, 341 (2014).
- ²¹R. Bhattacharya, B. Pal, and B. Bansal, *Appl. Phys. Lett.* **100**, 222103 (2012).
- ²²L. Lee, L. Zhang, H. Deng, and P.-C. Ku, *Appl. Phys. Lett.* **99**, 263105 (2011).
- ²³J. Christen and D. Bimberg, *Phys. Rev. B* **42**, 7213 (1990).
- ²⁴A. Yoshikawa, S. Che, W. Yamaguchi, H. Saito, X. Wang, Y. Ishitani, and E. Hwang, *Appl. Phys. Lett.* **90**, 073101 (2007).
- ²⁵C. Adelman, N. Gogneau, E. Sarigiannidou, J.-L. Rouviere, and B. Daudin, *Appl. Phys. Lett.* **81**, 3064 (2002).
- ²⁶S. Birner, T. Zibold, T. Andlauer, T. Kubis, M. Sabathil, A. Trellakis, and P. Vogl, *IEEE Trans. Electron Devices* **54**, 2137 (2007).